Timing is key in determining the impacts of demography on linked selection

Raul Torres[†,1], **Markus Stetter**[*], **Ryan HernandeZ**[†,1] **and**

Jeffrey Ross-Ibarra[*,‡,1]

[*]Dept. of Plant Sciences and Center for Population Biology, University of California, Davis, CA, USA, [†]Some other Department, Some other place, CA, USA, [‡]Genome Center, University of California, Davis, CA, USA

ABSTRACT Neutral genetic diversity across the genome is determined by the complex interplay of mutation, demographic history, and natural selection. While the direct action of natural selection is limited to functional loci across the genome, its impact can have effects on nearby neutral loci due to genetic linkage. These effects of selection at linked sites, referred to as genetic hitchhiking and background selection (BGS), are pervasive across natural populations. However, only recently has there been a focus on the joint consequences of demography and selection at linked sites on perturbing the patterns of neutral genetic diversity. Two recent studies investigating the impact of demography on BGS in the context of maize and humans found seemingly contradictory results. In order to reconcile differences observed in these studies, we conducted an extensive forward simulation study of BGS under a range of demographic models including population contractions, expansions, and bottleneck-expansion models of varying magnitudes and lengths of time. In each simulation, we measured relative neutral genetic diversity (π) and relative singleton density (ξ) over time as the population size changes. We found that both statistics vary dynamically over time, and that the initial dynamics after a population size change are often in the opposite direction of the long-term expected trajectory. Using these simulations and analytical calculations, we describe the temporal dynamics of neutral diversity in the context of selection at linked sites in populations of changing size and suggest a reconciliation of previously contradicting studies. Our work provides new intuition about why patterns of diversity under BGS vary through time as a function of demography and illustrates that classical models of BGS are poorly suited for predicting such patterns in the context of dynamic populations.

Introduction

The effects of natural selection and demography on neutral genetic diversity within populations have long been of interest in evolutionary and population genetics. Recent efforts in sequencing tens of thousands of genomes across a multitude of species have yielded new and valuable insights into how these two forces of evolution have shaped extant patterns of genomic variation. Yet, while the theoretical underpinnings of the effects of natural selection and demography on genetic diversity have been investigated for decades [1–9], detailed investigation into how they jointly act to create patterns of diversity in different populations remains lacking.

Both theory and empirical observation have long shown that patterns of neutral genetic variation can vary regionally across the genome as a function of recombination rate [1,10]. This is because natural selection operating on selected sites not only decreases genetic variation at the focal site but can also lead to decreases in nearby neutral genetic diversity due to genetic linkage [11]. These effects, known as genetic hitchhiking [1] (in which neutral variants rise to high frequency with adaptive variants) and background selection [6] (BGS; in which neutral variants are removed along with deleterious variants) can be widespread across the genome. Evidence for selection at linked sites has been found across an array of species, including *Drosophila melanogaster* [10,12–16], wild and domesticated rice [17,18], *Capsella* [19], maize [20], and humans [21–27].

Demographic change can also impact patterns of diversity across the genome. For example, neutral theory predicts that the amount of genetic diversity is proportional to a population's effective population size (Ne), such that changes in Ne should result in concomitant changes to diversity [28]. However, evidence suggests that such diversity also varies much less in magnitude across species when compared to their census population sizes [29,30]. One of the most common forms of a population size change is a population bottleneck, whereby populations suffer a large decrease followed by an expansion. Bottlenecks can occur via domestication events [31–34], seasonal or cyclical fluctuations in population size [35–38], and founder events [39–41]. Notably, while the rate of loss of diversity in response to a population contraction is quite fast, the recovery of diversity from a following population increase can be quite slow [42]. As a result, large contemporary populations may still yield patterns of low average genetic diversity if their population size was much smaller in the recent past. In humans, this is clearly evident in European and Asian populations due to the out-of-Africa bottleneck [43].

Because selection at linked sites and demography are both pervasive forces across a multitude of species, the characterization of how these two forces interact with one another is necessary in order to develop a full picture on the determinants of neutral genetic diversity. The efficiency of natural selection scales proportionally with Ne and the impact of selection at linked sites on neutral diversity is likely to be greater in larger populations and lower in smaller populations [5,11,44], although the rate of change for lowered diversity may diminish as populations reach larger and larger sizes [45,46]. Further, demographic changes can also increase (in the case of bottlenecks) or decrease (in the case of expansions) the rate of drift. It is therefore plausible that the rate at which diversity at a neutral locus is perturbed

by selection at linked sites could be highly dependent on both the current as well as long-term Ne of the population. This competition between "genetic draft" (which increases with N) and genetic drift (which decreases with N) may be a key contributor to the limited range of diversity observed among species despite much larger observed differences in census size [44–46]. However, selection at linked sites alone may not be sufficient to explain the observed discrepancy between observed diversity and census populations sizes [47], and the action of both demography and selection at linked sites in concert may provide a better model.

Many models of selection at linked sites were also formulated with the assumption that the population is large enough (or selection strong enough) such that mutation-selection balance is maintained [6,48,49]. However, non-equilibrium demographic change may break such assumptions and forces other than selection may drive patterns of variation in regions experiencing selection at linked sites. For example, during the course of a population bottleneck, genetic drift may transiently dominate the effects of selection at many sites such that traditional models of selection will poorly predict patterns of genetic diversity. But linked selection may also exacerbate the impact of genetic drift, resulting in even greater losses than expected by the action of demography alone. A recent review by Comeron et al. 2017 [50] included a cursory investigation into the impact of demography on diversity in regions under BGS and suggested a dependency on demographic history. Recent empirical work in maize and humans has also demonstrated a strong interaction between demography and selection at linked sites [20,51]. But these papers also demonstrates the need for a deeper understanding of the interaction between demography and selection at linked sites, as the two studies come to opposing conclusions about the impact of population bottlenecks and expansion on patterns of diversity in regions affected by selection at linked sites.

In order to more fully explore the joint consequences of demography and selection at linked sites, in this study we conducted extensive simulations of different demographic models jointly with the effects of BGS. We find that the time span removed from demographic events is critical for populations experiencing non-equilibrium demography and can yield contrasting patterns of diversity that reconciles apparently contradicting results from maize and humans [20,51]. Additionally, the sensitivity of genetic diversity to demography is dependent on the frequency of the alleles being measured, with rare variants experiencing more dynamic changes through time.

Our results demonstrate that traditional models of selection at linked sites may be poorly suited for predicting patterns of diversity for populations experiencing recent demographic change, and that the predicted forces of BGS become apparent only after populations begin to approach equilibrium. Importantly, even simple intuition about the effect of selection at linked sites may lead to erroneous conclusions if populations are assumed to be at equilibrium. These results should motivate further research into this area and support the use of models that incorporate the joint effects of both demography and selection at linked sites.

Materials and Methods

Simulation model

We simulated a diploid and randomly mating population using fwdpy11 v1.2a (*https://github.com/molpopgen/fwdpy11*), a Python package using the fwdpp library [52]. Selection parameters for simulating BGS followed those of Torres et al. 2018 [51], with deleterious variation occurring at 20% of sites across a 2 Mb locus and the selection coefficient, s, drawn from two distributions of fitness effects (DFE). Specifically, 13% of deleterious sites were drawn from a gamma distribution (parameters: mean = α/β, variance = α/β^2) parameterized Gamma($\alpha = 0.0415$, $\beta = 80.11$) and seven percent from a distribution parameterized Gamma($\alpha = 0.184$, $\beta = 6.25$). These distributions mimic the DFEs inferred across non-coding and coding sites within the human genome [53,54]. Fitness followed a purely additive model in which the fitness effect of an allele was 0, 0.5s, and s for homozygous ancestral, heterozygous, and homozygous derived genotypes, respectively. Per base pair mutation and recombination rates also followed those of Torres et al. 2018 51 and were 1.66×10^{-8} and 8.2×10^{-10}, respectively. We also included a 200 kb neutral locus directly flanking the 2 Mb deleterious locus in order to observe the effects of BGS on neutral diversity. For all simulations, we simulated a burn-in period for 10N generations with an initial population size of 20,000 individuals before simulating under 12 specific demographic models. The demographic models included one demographic model of a constant sized population (model 1) and eleven non-equilibrium demographic models incorporating both bottlenecks and expansion (models 2-12; Figures **??-??**; Table **??**). For each demographic model, we also conducted an identical set of neutral simulations without BGS by simulating only the 200 kb neutral locus. Each model scenario was simulated 5,000 times.

Diversity statistics and bootstrapping

After the burn-in period, we measured genetic diversity (π) and singleton density (ξ; the number of singletons observed within a locus) within 10 kb windows across the 200 kb neutral locus every 50 generations using a random sample of 400 chromosomes. We measured π and ξ for each demographic model by taking the mean of these values across each set of 5,000 replicate simulations. For neutral simulations, we annotated π and ξ as π_0 and ξ_0, respectively. We took the ratio of these statistics (i.e., π/π_0 and ξ/ξ_0) in order to measure the relative impact of BGS within each demographic model. We bootstrapped the diversity statistics by sampling with replication the 5,000 simulated replicates of each demographic model to generate a new set of 5,000 simulations, taking the mean of π and ξ across each new bootstrapped set. We conducted 10,000 bootstrap iterations and generated confidence intervals from the middle 95% of the resulting bootstrapped distribution.

Calculations of expected BGS

To calculate the predicted can we say instantaneuos? π/π_0 given the specific N_e at each time point for each demographic model, we used equation 14 of Nordborg et al. 1996 [7], but modified it accordingly to incorporate two gamma distributions of fitness effects. Additionally, in order to properly model our simulations, we only calculated the effects of BGS on one side of the selected locus. This resulted in the following modified equation:

$$\frac{N_e}{N} \equiv \frac{\pi}{\pi_0} =$$

$$exp\left(-\frac{U_T}{2R}\int_C^\infty \frac{1}{s}\left\{\int_0^R \frac{dz}{[1+r(z)(1-s)/s]^2}\right\}\Gamma(s,\alpha_T,\beta_T)ds\right) \times$$

$$exp\left(-\frac{U_B}{2R}\int_C^\infty \frac{1}{s}\left\{\int_0^R \frac{dz}{[1+r(z)(1-s)/s]^2}\right\}\Gamma(s,\alpha_B,\beta_B)ds\right)$$

Here, *R* is the total length in cM or? of the selected locus, *U* is the total deleterious mutation rate across the selected locus, $r(z)$ is the genetic map distance between a neutral site and a deleterious mutation, and *s* is the selection coefficient of a deleterious mutation. The left side of the equation models the effects of BGS according to the gamma DFE inferred by Ref. [53] (represented by $\Gamma(s, \alpha_T, \beta_T)$) and the right side of the equation models the effects of BGS according to the gamma DFE inferred by Ref. [54] (represented by $\Gamma(s, \alpha_B, \beta_B)$).

Because N_e is not explicitly included in this model of BGS, we followed previous workers [12,55] in trtuncating selection at some value *C*, such that $C = \gamma/2N_e$ (represented in the integral $\int_C^\infty$). Here, *C* represents the minimum selection coefficient which is treated as deleterious for the model and γ represents the population scaled selection coefficient ($\gamma = 2N_e s$) that determines the value of *C*. Thus, this step excludes effectively neutral mutations from the model that should not contribute to BGS. This truncation step also affects the values used for *U* in the above equation, resulting in specific values of *U* for each DFE. We simulated different population sizes under our BGS simulation model to see how well the modified Nordborg model fit populations of different N_e for different values of γ (Figure S3). We used a $\gamma = 0.15$ because this provided the best estimate of π/π_0 for the starting N_e of our demographic models (i.e., $N_e = 20,000$). While this value provides a coarse estimate for the effects of BGS on π/π_0 for a particular N_e, it will overestimate the effects of BGS for smaller N_e (Figure S3).

Results

Background selection under instantaneous population size change

We first present the joint effects of demography and bacgkround selection (hereafter, BGS) under simple demographic models with a single instantaneous change in size (models 2-4; Figure **??**). While our simulation model incorporated a 200 kb neutral region, we first focused on patterns of diversity generated within the 10 kb window nearest to the 2 Mb locus experiencing purifying selection, as this is where BGS is strongest. Doing so allowed us to observe any change in the dynamics of π and ξ as they approached new population equilibria resulting from a change in size. In the simple bottleneck models (models 2-3) we observed the expected strong decrease in ξ and π following population contraction in both models of BGS and neutrality (Figure 1). Similarly, we observed the expected rapid increase in ξ compared to π in our model of a simple population expansion (model 4; Figure 1). could probably ditch the legend inset here since the caption provides colors In all cases, values of ξ and π were consistently lower in models with BGS, consistent with the known effects of BGS on diversity (Nordborg *et al.* 1996).

To examine the interaction of demography and selection observed in empirical data (Beissinger *et al.* 2016; Torres *et al.* 2018), we normalize π and ξ in models of BGS by their equivalent statistics generated under the same demographic model in the absence of any selection (π_0 and ξ_0). We observed that π/π_0 and ξ/ξ_0 were dynamic through time in response to demography, with changes occurring to both their magnitude and direction (Figure 2). Moreover, changes to ξ/ξ_0 occurred more rapidly through time when compared to π/π_0. For example, in model 2 we observed a dip and rise in the ξ/ξ_0 statistic (i.e., relative to model equilibrium model 1) within the first $\approx 0.1N_{anc}$ generations (N_{anc} refers to the N_e of the population in the ancestral generation of the model). Yet, for the same model, π/π_0 remained
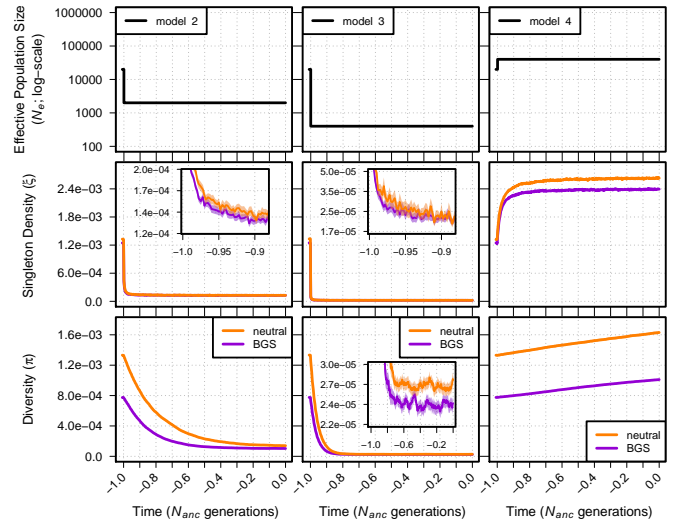

Figure 1 Singleton density (ξ per site) and diversity (π per site) for models 2-4. The top panel shows each demographic model; time proceeds forward from left to right and is scaled by the N_e of the population at the initial generation (N_{anc}). Diverstiy statistics are shown for neutral simulations (orange lines) and simulations with BGS (violet lines). Insets show diversity using a log scale for improved detail. Envelopes are 95% CIs calculated from 10,000 bootstraps of the original simulation data.

depressed for over $0.5N_{anc}$ generations (Figure 2). Similar patterns were observed for model 3, which experienced a greater reduction in size, although this pattern is less clear due to the greater sampling variance exhibited between successive time points for the ξ/ξ_0 statistic. This increased variance may stem from the fact that rare variants are especially sensitive to loss during a population reduction [9] and fewer number of them remain in the population following the size change (Figure 1). However, as expected for a population suffering a smaller reduction, lower sampling variance for ξ/ξ_0 was observed across each successive time point in model 2. is this sentence necessary?

However, when we observed the relative increase of ξ and π under BGS versus neutrality by measuring ξ/ξ_0 and π/π_0, we saw that the increase for ξ and π occurred at a greater rate under BGS (Figure 2). Thus, the patterns of ξ/ξ_0 and π/π_0 that manifested occurred in opposite directions from what we observed in demographic models with a population contraction – namely a transient increase in ξ/ξ_0 and a sustained increase in π/π_0. The latter pattern occurred despite the expectation of a decrease in π/π_0 from the Nordborg model, which would have been generated by more efficient purifying selection accompanying a larger N_e.

The more sensitive and rapid response to population increase under BGS recapitulated the faster approaches to equilibrium that were exhibited in the contraction models. Intuitively, these faster approaches to new equilibrium levels under BGS in response to size changes make sense if we consider the fact that the distance between initial and final equilibrium diversity levels for both π and ξ are closer to one another under BGS when compared to neutrality (Figure S6; Table 2-3). This provided a potential explanation for why we observed the specific dynamics of π/π_0 immediately following a size change. This argument likely does not hold for model 4 because, due to its higher N_e,
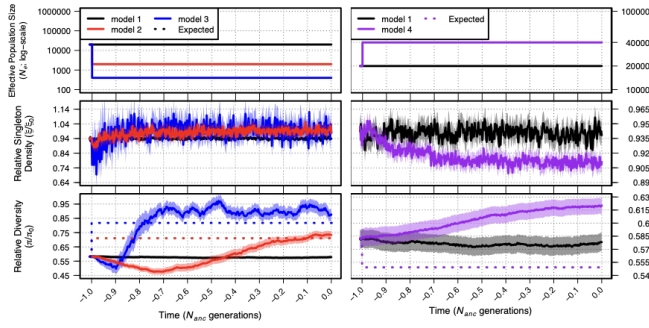
Figure 2 Relative singleton density (ξ/ξ_0) and relative diversity (π/π_0) across time for demographic models 1-4. Top panel shows each demographic model (time proceeds forward from left to right, scaled by the Ne of the population at the initial generation ($_{Nanc}$)). Black lines show ξ/ξ_0 and π/π_0 from simulations of a constant sized population (model 1). Dotted lines in the bottom panel show the instantaneous expectation of π/π_0 from Eq. (14) of Nordborg *et al.* (1996) given the specific selection parameters and the instantaneous N_e at each time point. See Table 1 for demographic model parameters. Envelopes are 95% CIs calculated from 10,000 bootstraps of the original simulation data.

it is unlikely that equilibrium has yet been reached. However, the observation of an increase in π/π_0 for model 4 did provide supporting evidence that a faster approach to equilibrium under BGS still existed under an expansion model. Indeed, moderl 4 π under BGS changed more quickly than under neutrality (Figure S9). Presumably, this also indicates that π under BGS will reach a new equilibrium first, at which point π/π_0 will begin a downward trajectory in response to π continuing to increase under neutrality but π under BGS remaining at a constant equilibrium. This is a likely outcome if the qualitative changes in ξ/ξ_0 foreshadow the future dynamics of π/π_0. The end result would also include a decrease in π/π_0 relative to its initial starting point, with π/π_0 eventually reaching a value close to its expectation (Figure 2; dotted lines). Although we foresee no reason why this prediction should not hold true, more extensive simulations will be necessary to confirm this.

Changes in population size should lead to changes in the rate of genetic drift and the efficacy of natural selection and, thus, changes in the magnitude of BGS across time. Indeed, in equilibrium contions, the classic model of BGS (Nordborg *et al.* 1996) predicts that smaller populations will experience weaker BGS (with higher π/π_0 and ξ/ξ_0). To compare these prediction to those of our simple o test for this type of outcome, we calculated the predicted π/π_0 given the specific N_e at each time point using the BGS model of (we will refer to this as the classic model; see Materials and Methods). When comparing the expectation of π/π_0 from the classic model with our simulation data, we observed qualitatively opposite patterns (Figure 2; bottom panel). In both models 2 and 3, the Nordborg model predicted a higher value for π/π_0 immediately following the population contraction, which was in contrast to the observed transient drop in π/π_0 for both models. While the effects of BGS should be attenuated in populations with lower N_e (because the efficacy of purifying selection is weakened), the drop in π/π_0 instead demonstrated that the populations were dominated by the effects of allelic loss, which is expected for populations suf-

fering a strong bottleneck. Additionally, more rapid effects were observed for model 3s despite the fact that the expectation of π/π_0 for model 3 was actually higher than for model 2. These observations made it clear that effects of BGS on π/π_0 immediately following a reduction in N_e were not driven by a change in the efficacy of natural selection from population decline, but rather by the increased sensitivity of allelic loss within these regions – with greater rates of loss accompanying greater reductions in population size. The diversity-reducing effects of BGS have often been modeled as a reduction in N_e [56], which has been observed to increase sensitivity to drift for populations experiencing recent bottlenecks [51] (though we caution that effects of BGS on the SFS cannot be simplified to this extent [57]). These patterns were made evident when observing the more rapid relative decrease in diversity in our selection models with BGS versus neutrality. When compared to their initial equilibrium starting points, π under BGS suffered faster rates of loss compared to the neutral case for both models (Figure S9), with the fastest rates of loss accompanying larger reductions in N_e (i.e., model 3). Importantly, these results demonstrated that classical models that predict the impact of BGS on π/π_0, such as the Nordborg model, implicitly assume an equilibrium population at mutation-selection balance [58] and are inappropriate for predicting true patterns of genetic diversity for populations that have udnergone recent size changes.

Even though ξ/ξ_0 and π/π_0 experienced drops immediately in response to the population reductions of models 2 and 3, these patterns of reduced ξ/ξ_0 and π/π_0 reversed themselves through time and, in the case of π/π_0, approached the expectation predicted by the Nordborg model. These dynamics occurred more quickly for ξ/ξ_0, which was expected since approaches to equilibrium are more rapid for rare variants relative to common variants. Additionally, the approaches to equilibrium occurred fastest for model 3, which also suffered the larger population size reduction (Figure 1). This faster approach was also not unexpected since, in general, the time to equilibrium is scaled by N_e [28,58] and changes resulting in smaller N_e (e.g., model 3) should also result in shorter times towards new population equilibria. Thus, despite the demographic change resulting in immediate decreases to ξ/ξ_0 and π/π_0, patterns of relative diversity in populations suffering a contraction eventually approached their expected higher equilibrium values under weakened BGS, with rates dependent on the frequency of the alleles being observed and the magnitude of the population reduction. This was evident from the fact that the final π/π_0 values for models 2 and 3 were within close approximation of the Nordborg model. However, we note that this expectation underestimated π/π_0 for model 3 because the threshold of $s < 0.15/2N_e$ was likely not conservative enough to ignore deleterious mutations that behave neutrally under the low N_e size of 400 for that model.

Simulations of BGS and demography – bottleneck-expansion models

We built upon the simple two epoch demographic scenarios to test more complex demographic scenarios and their effects on patterns of diversity under BGS. Specifically, we incorporated a bottleneck-expansion model where we simulated a population undergoing a contraction similar in size to models 2 and 3, but with a subsequent expansion to 400,000 individuals by the final generation. Although we vary the time length of the contraction and expansion events (see Table 1), these bottleneck-expansion models qualitatively match the demography of previous empiri-

cal studies investigating the impact of BGS in dynamic populations [20,51]. They also helped to glean information about which particular demographic events — contractions or expansions — dominate the overall patterns that we witnessed for the two epoch models described previously.

For the demographic models in which the bottleneck event began -1.0 N_{anc} generations in the past and was followed by immediate expansion (models 5-6), we observed transient decreases in ξ/ξ_0 and π/π_0, recapitulating the dynamics observed for models 2 and 3 (Figure 3). Similar to models 2 and 3, we also observed approaches to higher values of π/π_0 later in their demographic histories, consistent with the effects of weakened BGS as a result of the initial population decline. This was in contrast to the decreasing π/π_0 expected for an expanding, larger population (Figure 3; dotted lines). The approach to higher π/π_0 values later in the demographic model also occurred more rapidly for model 6 than model 5. Thus, as was shown when comparing model 3 to model 2, the time to equilibrium after a size change is highly dependent on N_e and occurs more quickly for populations suffering larger reductions. The fact that these patterns of increasing π/π_0 exist despite the population expansion events of models 5 and 6 also demonstrates the dominant effects that a population decline has on patterns of diversity under selection at linked sites.

While the population expansion eventually did have an effect on increasing π under both BGS and neutrality after the initial reduction in size, this increase occurred at a higher relative rate under BGS and was further accelerated by larger reductions in population size. This is evident in Figure S7 where we compared π relative to its initial value through time. There, we observed a sharper increase in π under BGS following its minimum point for model 6 when compared to model 5. However, for both models, the faster rate of recovery of π under BGS in response to the expansion also ensured that π/π_0 continued to remain higher in later generations. So while bottlenecks led to a sharper rate of decrease in π under BGS when compared to neutrality, they also aided in a faster rate of recovery during the expansion, thereby leading to an increase in π/π_0 in the face of growth and mimicking patterns evident for models with no expansion. The fact that the approach to higher π/π_0 occurred *despite* the increasing population size of both demographic models clearly demonstrated that patterns of π/π_0 were primarily being driven in response to earlier demographic events (i.e., the initial population contraction). Yet the stronger action of BGS in response to population expansion should eventually arise for both models and is suggested by the decreasing π/π_0 predicted by the Nordborg model (Figure 3; dotted lines). Such patterns may take much longer to manifest than the time span we have simulated here if approaches to equilibrium take on the order of $4N_e$ generations [28,58].

Observations of the dominant impact of genetic drift and weakened BGS following a population reduction were also apparent when measuring patterns of π/π_0 in models that had a more sustained contraction (i.e., models 7 and 8). There, a decline in N_e was sustained for an additional 0.5 N_{anc} generations before the expansion event began (Figure S2). For these models, the rise of π/π_0 resulting from weakened BGS occurred more quickly than for their counterpart models with an immediate expansion (Figure S3). For example, the inflection point at which π under BGS surpassed π under neutrality occurred at -0.305 and -0.848 N_{anc} generations for models 7 and 8, respectively (Figure S7). For models 5 and 6, these inflection points occurred later in

time at -0.235 and -0.785 N_{anc} generations, respectively. Further, the final π/π_0 values for models 7 and 8 were 0.643 and 0.887 but for models 5 and 6, they were only 0.631 and 0.860. Thus, the sustained lower N_e of models 7 and 8 aided in accelerating the approach to the new equilibrium established by population reduction. This provided further evidence for the dominant role that population bottlenecks have for patterns of diversity under BGS, even when populations expand past their ancestral size.

It is possible that the expansion itself has contributed to the rise in π/π_0 for models 5-8, as was seen for model 4. However, this is unlikely to be the case because the rise in π/π_0 occurred fastest for models 7 and 8, which had a delayed onset of expansion. Second, this rise occurred faster still for models 2 and 3, which had no expansion in size. There, the inflection point at which π under BGS surpassed π under neutrality occurred at -0.44 and -0.865 N_{anc} generations for models 2 and 3, respectively (Figure S9). Rather, the population expansion of models 5-8 appeared to retard the approach to equilibrium in response to their size reductions, thus preventing π/π_0 from attaining higher values. When comparing each respective model's maximum π/π_0, we observed that models 2 and 3 both had the highest values given their respective population reductions to 2,000 and 400 individuals ($\pi/\pi_0 = 0.738$ and 0.972, respectively; Figure 1). This was followed by models 7 and 8 ($\pi/\pi_0 = 0.644$ and 0.887, respectively) and finally, by models 5 and 6 ($\pi/\pi_0 = 0.631$ and 0.861, respectively; Figure 3). Thus, those models experiencing the shortest amount of time at reduced population sizes saw the lowest rises in π/π_0. For models 5-8, though, π/π_0 was still approaching higher values since these models were not at equilibrium after 1.0 N_{anc} generations. It is likely that π/π_0 for these models would attain even higher values if their demographic histories were extended.

In contrast to π, the loss and gain of ξ and change to ξ/ξ_0 in response to the bottleneck-expansion models was much more rapid and dynamic through time. This was expected since rare variants (e.g., singletons) are more likely to be lost during a contraction, and during an expansion injection of new mutations fill these bins in the SFS first. For models 5 and 6, we witnessed a very brief dip in ξ/ξ_0, resulting from a greater relative decrease in ξ under BGS when compared to neutrality (Figure 3; Figure S7). Following this dip, ξ under BGS increased at a relatively faster rate than ξ under neutrality, resulting in a higher ξ/ξ_0 relative to their initial values (Figure S7). Similar patterns were also seen for models 7 and 8 (Figure S3, Figure S7). Qualitatively, these first directional changes in ξ/ξ_0 matched those of π/π_0, but occurred over a much shorter time span. These changes were likely a consequence of regime change from the dominance of genetic drift immediately following the population reduction to the dominance of weakened BGS from a reduced N_e. This was previously exhibited by models 2 and 3 and additional evidence for this was provided by the observation that changes in the magnitude of ξ/ξ_0 were greater for model 6 and model 8 than for model 5 and model 7 (i.e., greater for models suffering larger reductions in N_e).

Because the dynamics of rare variants are more sensitive to demography, we also witnessed another change in the direction of ξ/ξ_0 that was not observed for π/π_0. Following an increase in ξ/ξ_0 above its initial point from weakened BGS, we saw a decrease later in time, with ξ/ξ_0 falling below that initial point by -0.2 N_{anc} generations (Figure 3, Figure S3). This last decrease in ξ/ξ_0 could not have resulted from an increased sensitivity to drift because the population sizes were larger during this

phase of the demography (79,636 N_e and 57,722 N_e at -0.2 N_{anc} generations for models 5 and 6, respectively). Rather, BGS appeared to act more strongly in these later generations and, thus, limited ξ relative to its value under neutrality. Supporting this, we observed a slower rate of increase in ξ under BGS towards the very end of the expansion for models 5-8 (Figure S4; Figure S7). Finally, we observed that the final ξ/ξ_0 value for model 5 was lower than for model 6 (0.881 vs. 0.893) and the final ξ/ξ_0 value for model 7 was lower than for model 8 (0.879 vs. 0.896) (Figure S3). This may have resulted from the fact that models 5 and 7 had higher long term N_e and experienced a concomitantly stronger amount of BGS throughout their history due to their shallower population bottlenecks.

We also ran a set of simulations with demographic histories simulating the effects of more recent bottlenecks on patterns of π/π_0 and ξ/ξ_0 (models 9-12; Figure S2). These models were similar to models 5-8, with identical starting and ending population sizes and population size reductions. For these models, we observed similar patterns in response to the population reductions seen in the previous models. In all cases, π/π_0 suffered a decrease, which was once again in contrast to the expectation given by the Nordborg model (Figure S3). Also similar to the previous models, ξ/ξ_0 for models 9-12 suffered a transient decrease followed by a recovery over its initial value. For models 9 and 10, which both had an immediate expansion following their size reductions, the magnitude of loss for π and ξ was less than for their counterpart models – models 5 and 6 (compare Figure S4 to Figure S5). This result likely stemmed from the higher rate of population growth necessary to end at a size of 200,000 individuals over the course of 0.1 N_{anc} generations for models 9 and 10, which mitigated the greater loss of π and ξ exhibited by models 5 and 6. Additionally, the decrease in π/π_0 was less for models 9 and 10 when compared to models 5 and 6. After 0.1 N_{anc} generations, π/π_0 was 0.545 and 0.492 for models 5 and 6, respectively but 0.573 and 0.541 for models 9 and 10, respectively (Figure S3). This demonstrated the effects of the greater rate of expansion on limiting the sensitivity to drift in regions of BGS. Further, for models 11 and 12, which had a delayed expansion, measures of π/π_0 were also lower than for models 9 and 10 after 0.1N_{anc} generations, exhibiting values of 0.542 and 0.527, respectively (Figure S3). These models also clearly demonstrated the feature of ξ under BGS not only declining more quickly in magnitude immediately following the population contraction but also recovering more quickly once it reached its minimum, thus displaying the more rapid behavior characteristic of patterns of diversity under the effects of BGS and demography. Specifically, when comparing ξ under BGS to ξ under neutrality, ξ under BGS in the final generation was relatively higher than its initial value (Figure S8). This caused the elevated ξ/ξ_0 exhibited in the final generation of models 9-12 (Figure S3).

Because the history of models 9-12 only lasted 0.1 N_{anc} generations, we also observed much more limited dynamics of π/π_0 and ξ/ξ_0. Specifically, π/π_0 did not recover above its initial starting point by the final generation and ξ/ξ_0 did not decrease in response to the population expansion, but rather continued to remain elevated (Figure S3). These features are important because they demonstrated that qualitatively similar demographic events, such as the bottleneck-expansion model shared by models 5-8 and 9-12, can yield opposite trends in statistics used as proxies for measuring the intensity of BGS. Thus, the resulting effects on patterns of relative diversity under BGS depend on

how far removed the point of observation is from a particular demographic event. Such patterns also help to reconcile the qualitatively different observations yielded by previous studies [20,51] (discussed further below).

Patterns of π/π_0 and ξ/ξ_0 across 200 kb neutral region

We also measured patterns of π/π_0 across time for the entire 200 kb neutral region. Doing so showed the characteristic "trough" structure of increasing relative diversity as a function of genetic distance from the focl locus under selection (Figure 4, Figures S10-S20). For the two-epoch models with a population contraction (models 2-3) we observed that the slope of the trough became more shallow through time, with the difference between the closest 10 kb bin and farthest 10 kb bin from the 2 Mb selected locus decreasing between the initial and final generations (Figures S10-S11, Table 4). Thus, the impact of population contractions on mitigating the effects of BGS resulted in larger shifts of π/π_0 in regions of the genome already under the strongest amount of BGS. This makes sense since regions farther removed from loci under purifying selection (i.e., under weaker effects of BGS) have values of π/π_0 closer to the neutral expectation of 1. Thus, the upper bound for change in π/π_0 will be more limited there compared to regions more proximal to a selected locus. However, the decrease in the slope of the trough was initially minimal and only accelerated after π/π_0 across the 200 kb region reached its minimum values (Table 4). This provided further evidence for the dominant effects of drift and allelic loss on driving the initial decrease in π/π_0 immediately following a population contraction, which should have unbiased effects across all bins within the trough. During the subsequent recovery to higher values of π/π_0, we saw smaller differences arise between the nearest and farthest 10 kb bins, demonstrating the expected weakening effects of BGS following a population decline. This weakening of the trough structure was also most apparent for model 3, with patterns of π/π_0 appearing essentially flat across the 200 kb region in the final generation (Figure S11).

We observed similar patterns for the bottleneck-expansion models that lasted 1 N_{anc} generations (Figures S13-S16). Notably, among those models, the slope of the trough became more shallow for models 6 and 8 which were also the models suffering the deepest reductions in size (Figures S14, S16; Table 4). The fact that the trough structure for models 5 and 7 was better maintained showed that the population expansion following the reduction in size kept BGS stronger through time relative to models with the same decline in size but without a recovery (e.g., model 2). Models lasting 0.1 N_{anc} only captured the decrease of π/π_0 due to drift and saw very little difference develop across their troughs (Figures S17-S20). Similarly, for model 4, the trough structure remained unchanged throughout its demographic history (Figure S12).

Finally, repeating the same analysis across the 200 kb regions for ξ/ξ_0 yielded no discernible patterns. Troughs were slightly apparent for the final generations of some models (i.e., models 5 and 7), but the stochasticity between windows for ξ/ξ_0 swamped any obvious patterns across the 200 kb region through time. Since ξ/ξ_0 is already less affected (and, thus, closer to 1) than π/π_0 because BGS perturbs common frequency bins of the SFS more than rare ones [57], any signal using rare frequency bins will be inherently more difficult to capture across differing magnitudes of BGS. However, more extensive simulations may help to uncover such patterns.

Discussion

Conclusion

Recently, two empirical investigations into the joint impacts of demography and selection at linked sites in the context of BGS yielded interesting and intuitive, albeit contradictory, observations. Beissinger et al. [20] conducted a study across 36 samples from maize and its wild progenitor teosinte. They found that patterns of relative genetic diversity (i.e., π/π_0) across regions experiencing linked selection in maize, which underwent a demographic bottleneck during domesticaiton, were higher than in teosinte. They attributed this to the historically larger N_e of teosinte, which led to more efficient natural selection and thus a greater impact of BGS on neutral diversity. However, the contemporary population size of maize, a staple food crop grown world-wide, is now much larger than teosinte and should be experiencing stronger selection in its recent history. Supporting this hypothesis, relative singleton density of neutral sites in maize, which should reveal more recent signals of evolutionary history, was lower compared to teosinte. However, Torres et al. 2018 [51] revealed opposite patterns in humans. There, through a analysis of over 2,500 human genomes, they observed that relative genetic diversity (π/π_0) was lower in non-Africans, a population that has undergone a series of extensive population bottlenecks and exhibits a low long-term N_e, when compared to Africans. Additionally, relative singleton density was also higher in non-Africans. In conclusion, the authors attributed these patterns to a higher sensitivity to demography and drift in regions of selection at linked sites, thus yielding lower relative diversity in bottlenecked populations. They also concluded that the greater long-term N_e, and thus more effective purifying selection and greater BGS, of Africans has led to their observed lower relative singleton density.

While these patterns observed in maize and humans are seemingly in disagreement, important demographic details, such as the length of the population bottleneck and the time since the post-bottleneck population expansion began, may also be significant contributors to these results. As our simulations demonstrated, it is possible for two qualitatively similar demographic histories to yield opposite patterns if the window of time in which those patterns are observed are different. In the case of maize compared to teosinte, observations are being made at a time in which BGS is operating less effectively on removing average pairwise diversity (due to its lower long-term N_e) but more effectively on singletons (due to its higher contemporary N_e). But if this population had been sampled more closely to its population bottleneck event, observations of relative diversity may have been more aligned with what is currently observed for humans. The approximate number of generations removed from the domestication bottleneck event for maize is about 15,000 generations [20]. For humans, the approximate number of generations removed from the out-of-Africa bottleneck event is only 6,000 generations [51]. Therefore, it is not unreasonable to suspect that these different timespans contribute to the qualitatively different observations now being observed.

Importantly, these two studies provide striking examples of the importance of considering the impact of demography and time on extant patterns of diversity to avoid mis-attributing the underlying forces driving those patterns in regions experiencing selection at linked sites. Since the null expectation of a natural population should be that it is not at demographic equilibrium [59], alternative hypothesis testing on selection at linked sites should also include the effects of non-equilibrium demography and how they affect patterns though time. However, in the specific context of maize and humans, we also note that other details, such as the periodic bottlenecks suffered by non-Africans (which may have further accelerated drift) and the differences among the distribution of fitness effects for these two species, are equally important to consider and warrant further investigation as well.

Recent model development incorporating demography into models of BGS holds promise on generating demographically aware models on the effects of selection at linked sites in populations. In particular, results from Zeng 2013 [48], which formulated a simulation-based structured coalescent model of BGS with demography, also showed that demography can perturb levels of genetic diversity under BGS through time. In a separate study, an analytical model which is capable of incorporating changing demography was formulated and will prove more ideal for performing inference of selection at linked sites in dynamic populations [49]. Both of these models, though, are limited in their ability to accurately predict the effects of selection at linked sites when mutation-selection balance breaks down, which typically occurs when the population scaled selection coefficient, γ, approaches 1. In general, the deterministic approximation implicit for models of BGS may not be suitable for $\gamma \leq 3$ [56]. During the course of a bottleneck, as we have simulated here, γ is likely to fall below these thresholds and patterns of diversity may be more strongly affected by other processes such as genetic drift or the "interference selection" regime described in Good et al. 2014 [60]. For the case in which s is drawn from a skewed distribution, such as the gamma distribution, the deterministic approximation is further likely to break down when s is small. We attempt to limit these specific issues in the Nordborg model by simply truncating s so that predictions better match observed levels of BGS for various population sizes (albeit, under the additional assumption of demographic equilibrium). This simplistic approach may be suitable for other models of BGS, but as our results showed, it will likely provide only a coarse estimate for the prediction of diversity under BGS (Figure S21).

Finally, our results extend the recent debate on patterns of diversity in selected sites in non-equilibrium populations (especially in humans [61–64]) to patterns of diversity across neutral sites. For the specific case of selected sites, sites under strong selection are more sensitive to demographic change and will reach new equilibrium frequency levels more quickly than neutral sites or weakly selected sites [65–67]. As we have shown here in the context of neutral sites, because the underlying equilibrium frequency of neutral sites depends on the strength of selection at linked sites, demographic change will also result in distinct responses to their change in frequency. In addition, the rate of change will also depend on which bins of the SFS diversity is being measured with. Together, this results in the complex change of π/π_0 and ξ/ξ_0 through time that we observed from our simulations. This insight should provide caution, however, for studies attempting to uncover the action of natural selection by comparing sites within the genome since, even when controlling for the strength of BGS itself, frequencies of neutral sites may still be at different relative levels depending on the recent demographic history of the population.

Acknowledgments

References

Beissinger, T. M., L. Wang, K. Crosby, A. Durvasula, M. B. Hufford, *et al.*, 2016 Recent demography drives changes in linked selection across the maize genome. Nature plants **2**: 16084.

Nordborg, M., B. Charlesworth, and D. Charlesworth, 1996 The effect of recombination on background selection. Genetics Research **67**: 159–174.

Torres, R., Z. A. Szpiech, and R. D. Hernandez, 2018 Human demographic history has amplified the effects of background selection across the genome. PLoS genetics **14**: e1007387.
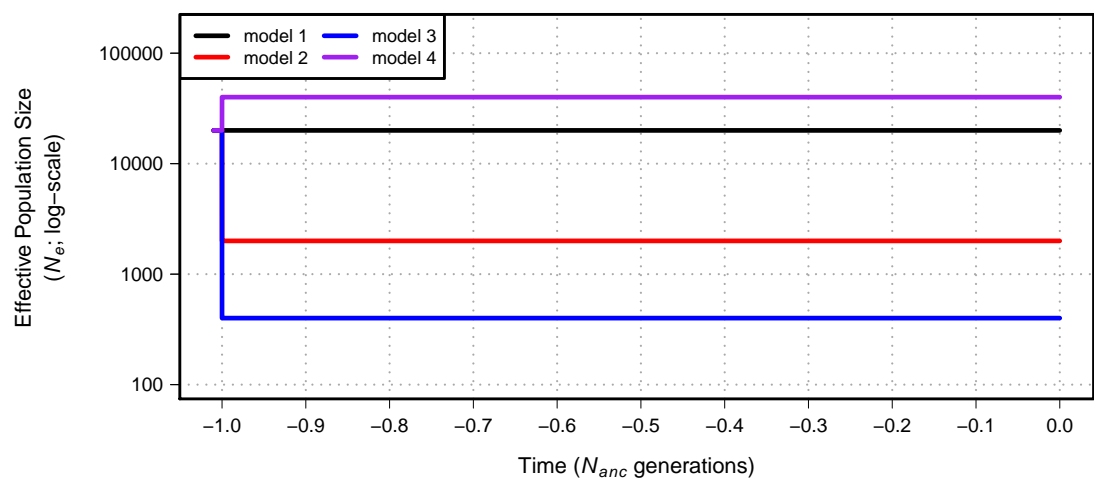
Figure S1 Demographic models 1-4 simulated in our study. Time proceeds forward from left to right and is scaled by the N_e of the population at the initial generation ($N_a nc$; 20,000 individuals). Demographic model 2 experiences a population contraction to 2000 individuals while demographic model 3 experiences a population contraction to 400 individuals. Demographic model 4 experiences a population expansion to 40,000 individuals. All population size changes are instantaneous for models 2-4. See Table **??** for additional model parameters.
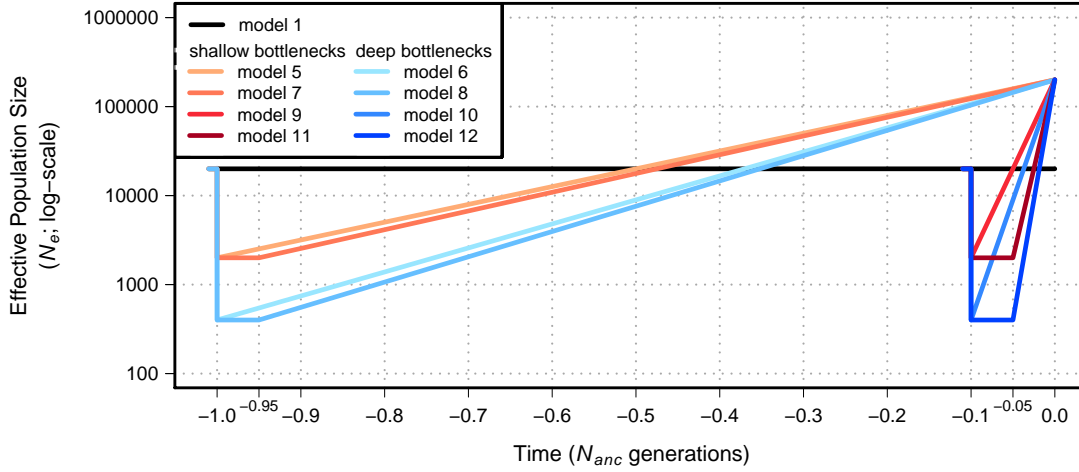
Figure S2 Demographic models 1 and 5-12 simulated in our study. Time proceeds forward from left to right and is scaled by the N_e of the population at the initial generation ($N_a nc$; 20,000 individuals). Demographic models experiencing a shallow bottleneck (models 5, 7, 9, and 11) experience a population contraction to 2000 individuals while demographic models experiencing a deep bottleneck (models 6, 8, 10, and 12) experience a population contraction to 400 individuals. After contraction, demographic models 5-12 undergo exponential growth to a final population size of 200,000 individuals. See Table **??** for additional model parameters.
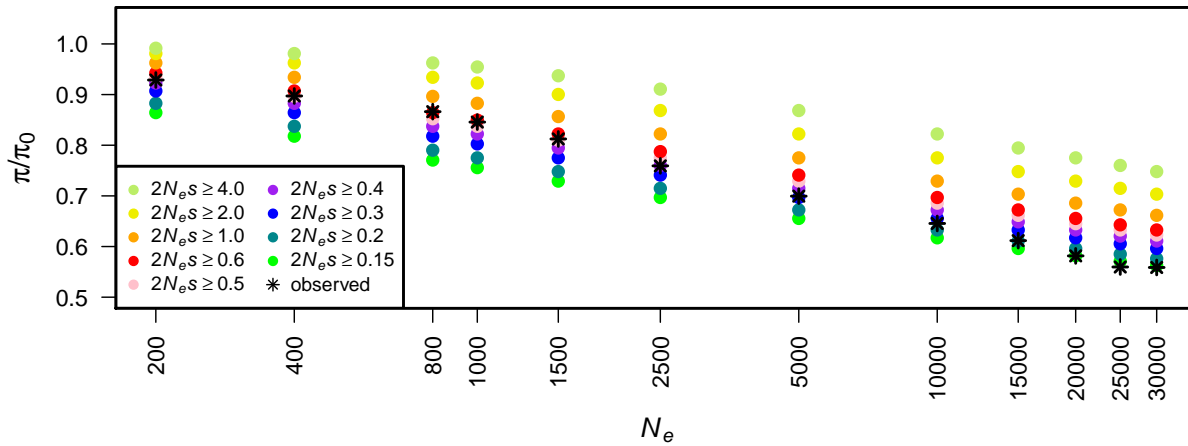

Figure S3 Estimate of $\pi\pi_0$ from the Nordborg model across different population sizes and different truncation thresholds on selection. Different γ values used to truncate s for the Nordborg model are shown in the legend ($2N_e s \geq \gamma$). Black stars represent the observed $\pi\pi_0$ from running simulations of BGS.